



Analysis of the Microstructure and Hardness of Flake Graphite Cast Iron Using the Barkhausen Noise Method and Conventional Techniques

Katarzyna Makowska¹ · Zbigniew L. Kowalewski²

Received: 24 October 2023 / Accepted: 13 March 2024
© The Author(s) 2024

Abstract

The new brake disc was evaluated for microstructure and hardness by the conventional destructive tests and non-destructive Barkhausen noise method (BNM). Ten non-destructive measurements were carried out in different areas of a brake disc, which were then cut out and made into metallographic test samples. Qualitative and quantitative analysis of graphite precipitates was performed to assess their volume in material matrix, anisotropy and size. Subsequently, graphs showing the relationships between selected stereological parameters of graphite precipitates and parameters determined from the RMS envelope of Barkhausen noise were elucidated. Similar relationships between hardness and parameters coming from non-destructive tests were carried out. Magnetic parameters that specified the size of a graphite precipitate was selected. In addition, repeatability studies using BNM were carried out in the areas of the material with the smallest and largest average size of graphite precipitates. A linear relationship between amplitude of BN and length of graphite flakes was found. The paper presents the possibilities of assessing the volume and size of graphite precipitates, as well as cast iron hardness using BNM.

Keywords Flake cast iron · Barkhausen noise · Brake disc · Non-destructive testing · Hardness

1 Introduction

Braking systems of most cars is based on brake discs, which are usually made of the gray cast iron. The microstructure of the gray cast iron determines strength, hardness, wear, noise and braking characteristics of the brake discs [1]. The brake disc wears itself too quickly if it is too soft. However, if the brake disc is too hard, it may be prematurely fractured [2]. Therefore, it is important to choose a tool that would be able to assess quickly the microstructure and hardness of the brake disc material. A grade of the cast iron is usually determined on the basis of Brinell hardness tests [3]. In addition, the hardness can serve as an indicator of selected tensile properties [3]. Also, the eddy current method is regarded as

the suitable technique for assessing the matrix composition of cast iron and its hardness, however, it is not widely used in the industry as yet [4]. Among non-destructive techniques also the ultrasonic methods were tried to be implemented for assessments of the graphite morphology, but unfortunately, their sensitivity was too low in the past and even nowadays is not sufficient [3]. Current achievements concerning the Barkhausen Noise Method (BNM) indicate, that it may be very suitable for the purposes mentioned above.

BNM may be used in analysis of the ferromagnetic materials, which consist of magnetic domains, only. Magnetic domains are micro-regions in which magnetization is homogeneous in terms of either the amplitude size or magnetization direction. A domain structure is created as the result of system striving for a state of the minimum internal energy. A division of the ferromagnet into domains causes a significant reduction of the demagnetizing field energy [5]. A formation preference of the domain structure over the state of uniform magnetization results from the fact, that the stronger exchange interactions are short-range, while the weaker dipole interactions are long-range and slowly decreasing with distance [5]. Therefore, it is possible to have in the ferromagnetics a domain structure and homogeneous or nearly uniform magnetization in the domains micro-areas.

✉ Katarzyna Makowska
katarzyna.makowska@wat.edu.pl

Zbigniew L. Kowalewski
zkowalew@ippt.pan.pl

¹ Faculty of Mechatronics, Armament and Aerospace, Military University of Technology, Military University of Technology, gen. Sylwestra Kaliskiego 2, 00-908 Warsaw, Poland

² Department of Experimental Mechanics, Institute of Fundamental Technological Research of the Polish Academy of Sciences, Pawińskiego 5B, 02-106 Warsaw, Poland

A number, size, and shape of the magnetic domains, and also, directions of their magnetization with respect to the crystallographic axes depend on the internal energy of the ferromagnet, which is the sum of five main components: exchange energy E_w , magnetostatic energy E_s , magnetocrystalline anisotropy energy E_a , magnetoelastic energy E_m and domain boundary energy E_d [6]. The exchange energy E_w is responsible for the formation of spontaneous magnetization in the ferromagnets. The magnetostatic energy E_s is related to the field demagnetizing the specimen. The magnetocrystalline energy E_a is the energy required to turn the domain spin systems away from the direction of easy magnetization. The magnetoelastic energy E_m is generated in a material under ferromagnetic stress as the result of magnetostrictive magnetoelastic strain. The domain boundary energy E_d depends on the number of domain boundaries in the material considered [6].

Barkhausen Noise (BN) is defined as a voltage signal that is generated during discontinuous domain wall movement in a changing magnetic field [7]. In the case of ferromagnetic material not magnetized by the external magnetic field, and moreover, not subjected to external stress, it consists of domains with the magnetic field directed along the magnetization axis, thus exhibiting the lowest energy of the magnetocrystalline anisotropy [6]. Magnetizations coming from the individual resultant domains are compensated because they are chaotically oriented relative to each other. An action of the external magnetic field on the ferromagnetic causes gradual reorientation of its domain structure. As the magnetic field increases, the value of magnetostatic energy E_s increases [6].

Magnetic domains with dipole moment directions close to the direction of the magnetic field, representing the region of lower hysteresis loop curvature for the range of lower magnetic field strengths, grow at the expense of the magnetic domains of direction basically different from that of the external magnetic field, which causes displacement of the domain walls, and simultaneously, activates a shift of the domain boundaries [6].

In the region of upper hysteresis loop curvature, the ferromagnet becomes saturated, i.e. the magnetization vectors of domains rotate from the easy magnetization axis direction to that of the external magnetic field, however, the domains do not change their volume. This is an energetically beneficial process despite the presence of magnetic anisotropy energy [6].

A smaller angle between the magnetization vector of domain and direction of the external magnetic field leads to the higher magnetic anisotropy energy that inhibits the domains rotation. Closing domains disappear due to the rotation process of the magnetization vector of domains [6].

The material can be magnetized only slightly after exceeding a certain value of the magnetic field strength, since the

magnetic saturation of the material was attained, that is, the areas of spontaneous magnetization were completely arranged. The processes of domain wall displacement as well as magnetization vectors rotation were completed [6]. In addition, there is a slight increase in magnetization for the strong magnetic fields due to the process of co-aligning the spin magnetic moments with the direction of external magnetic field. As a consequence, the magnetized material takes a microstructure of the specific grain size and specific internal defects such as non-metallic inclusions or internal discontinuities [6]. Domain walls are pinned temporarily by microstructural barriers to disable their motion, and are subsequently released abruptly in the magnetization cycle. It leads to discrete changes in local magnetization, which can be detected by means of a pick-up coil. Among many kinds of microstructural barriers the breaking domain wall movement, grain boundaries, precipitates, dislocations [8] and voids [9] can be distinguished.

The Barkhausen Noise Method (BNM) has been widely accepted in microstructural testing. For example, it can be employed to recognize different materials' structure, such as ferrite, pearlite, martensite, and ferrite with cementite [10]. The temperature of the steel tempering process after quenching can also be estimated on the basis of BN levels [11]. The volume of ferrite in the range from 3 to 48% was correlated with BN levels in the ferritic-martensitic steels [12]. The spheroidization process of AISI1060 ferrite-pearlite steel was successfully analysed by means of BNM in [13]. Moreover, Yamuara et al. [14] have established the relationship between the mis-orientation angle and BN.

Because BNM is very sensitive to microstructural changes, BN detection technology is also commonly used for identification of a grain size [14], texture [15] and material degradation [16]. Moreover, it has been discovered that the linearity effect of BN variations increases with the decrease of grain size [14]. The authors of [15] observed, that the peak heights of BN fingerprints increase with increasing of cold work percentage. According to [11], deformation process reduces grain size and creates dislocation cells in the material, which shortens the mean free paths of domain walls. In [16], the 5Cr–0.5Mo steel was subjected to creep at 600°C/60 MPa. The results of experiment showed, that in the early stages of damage BN decreases due to precipitation of new carbides that hinder the movement of domain walls. In the second stage of creep, as the carbides coagulate and the amount of obstacles decreases, BN increases. During the third stage of creep, the carbides continue to coagulate, and as a consequence, the mean free paths of domain walls increase, leading to BN increase. As voids in the material start to appear, a demagnetizing field starts to create itself too, and the noise slightly decreases [16]. The BNM for assessing the process of creep and plastic deformation was also described

in [17], while domain walls pinned by microstructural defects during different loading processes were presented in [18].

Also, attempts have been made to use the BNM to evaluate cast iron. Gür et al. [19] have found the relationship between the peak position of BNM and austempering time of ADI alloy [19]. Firstly, the peak position of BNM amplitude increases with the austempering temperature increase and attains a maximum during the austempering time. Such process occurs although the retained austenite content is higher for the upper bainite than that for the lower one [19]. This is because the BN parameters are determined mainly for a morphology of the bainitic ferrite [19]. The maximum peak position corresponds to optimal strength and ductility of the material. Subsequently, the peak position of BNM amplitude decreases during the heat treatment. A decrease of BN amplitude is connected with a decrease of bainitic ferrite volume fraction when the austenitizing temperature is increased [19].

In [20] the pearlite fraction was studied by using BNM on a set of GGG70 ductile cast iron inter-critically annealed at different temperatures. Linear relationship was found between root-mean-square (RMS) voltage of BN and pearlite fraction. As the pearlite content increased, the Barkhausen signal level also increased [20]. Moreover, linear relationship between RMS and hardness was determined [20]. It was stated, that with the RMS of BN value decrease, the hardness of GGG70 iron also decreases [20]. It was shown by Kiliçli et al. [20], that BN method may be used to control a microstructure and hardness of the ductile iron after technological processes.

Stupakov et al. [21] emphasised that the Barkhausen signal can be applied to detect the iron matrix structure of ductile cast iron. However, sensitivity for the graphite morphology observation was lower than that for the matrix variation evaluation [21]. The ability to distinguish differences in the cast iron matrix microstructure using BNM results from this technique sensitivity into dynamics of domain walls movements. In [22], it was confirmed using the Lorentz microscopy that domain walls can move freely through the ferrite, however, they are strongly pinned at the ferrite-pearlite boundaries. This means, that in the materials with a fully pearlitic microstructure, the movement of domain walls is even more difficult in the case of ferrite absence.

Gür et al. [23] tried to assess the microstructure of two-phase cast iron of the ferritic-martensitic matrix and spherical graphite. The authors found, that BN is very sensitive to Inter-critical Austenitizing Temperature ICAT, and thus, sensitive to pro-eutectoid ferrite volume fraction. The volume fraction of pro-eutectoid ferrite increases with ICAT increase at the expense of the martensite content. As a result, BN increases.

Altpeper [24] compared the amplitude of BN in white cast iron and structural steel in relation to the cementite content. The difference of BN level was significant after exceeding 30% wt. Fe_3C . In the range of up to 30% Fe_3C , the amplitude of BN increased slightly. Such range of the cementite

corresponded to a steel grade with structural components of ferrite, pearlite and secondary cementite. In the case of ferritic-pearlitic steel taken into account, the cementite was presented in pearlite. The higher content than 30% wt. Fe_3C corresponded to the formation of white cast iron components: ledeburite, pearlite and secondary cementite. In white cast iron a part of cementite was bound to pearlite, and the rest to ledeburite. Since cementite in white cast iron increased, the amplitude of BN increased significantly.

The domain wall behaviour in iron during magnetization cycle was described in detail by Buttle et al. [25]. According to [25] the irreversible motion of the domain walls at low intensity magnetic fields were almost entirely due to 180° domain walls type. In the case of higher intensity magnetic fields the 90° domain walls also gave an important contribution to BN, particularly near the “knee” regions of the hysteresis curve [25].

The publications referenced above deal with testing of the microstructure of various steels and grades of iron using BNM. However, no sufficient attention has been paid to the gray cast iron, which is a commonly used engineering material. Therefore, the goal of this work is focused on analysis of a diversity of the flake graphite sizes and hardness of the cast gray iron using BN analysis. BNM is presented as a potential inspection method to classify the grade of flake graphite in cast iron. Heterogeneously distributed graphite in the material may cause uneven development of its wear, and may also lead to damage in the further stage of its operation. Therefore, it is required to use a method that will allow to assess quickly and for a low cost the required quality of the flake cast iron products.

2 Material and Experimental Procedure

The experimental program contained 10 tests carried out on specimens cut out from a new, unexploited cast iron brake disc. Dimensions of all specimens were the same and characterized by length, width and height equal to 20 mm, 8 mm and 10 mm, respectively. They enabled the non-destructive measurements using a special head fitted to BN defectoscope. During manufacturing stage all the specimens were subjected to grinding on 320 and 1200 sandpaper in order to reduce their roughness.

In the next step of research procedure, BN was measured for all specimens fabricated. BNM belongs to the surface measurement techniques [26].

Magnetic tests were carried out using the MEB-4C measuring set (Fig. 1) equipped with a special head (Fig. 2). It consisted of a U-shaped core of electromagnets wrapped in the wound excitation coil. The pick-up coil was built-in to the sensor. A triangular waveform was applied. In the pick-up coil, a voltage signal was induced. To estimate an intensity of

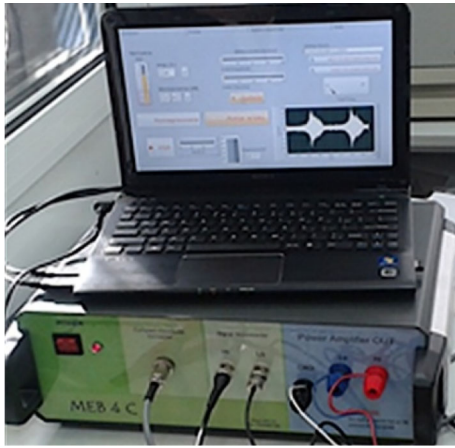


Fig. 1 BN defectoscope MEB-4C [17]

BN, the fast-variable component was separated by means of a high-pass filter $f = (0-500)\text{Hz}$. Analysis of this component provided data on the specimens' material structure. A slope of the magnetizing current 8 A/s and generator gain of 10 dB were used.

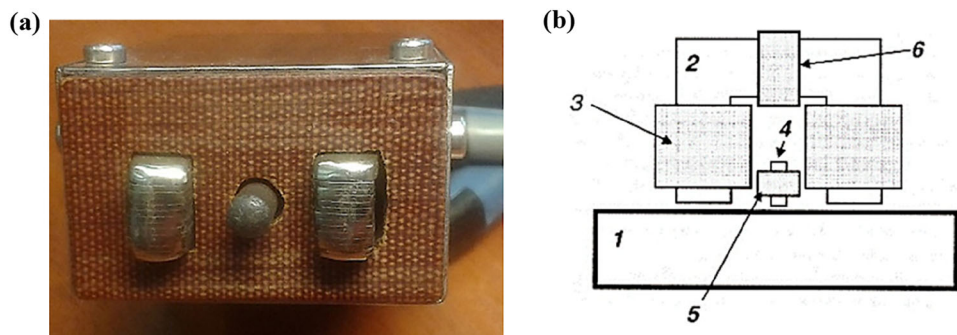
The envelopes of BN were calculated as RMS value of U_b according to the equation [2]:

$$U_b = \sqrt{\frac{1}{\tau} \int_0^\tau U_{ib1}^2(t) dt}, \tag{1}$$

where, U_b [V] is the root mean square of the coil output voltage; U_{ib1} [V] is the fast-variable component defining voltage separated by means of the high-pass filter from the induced voltage in the pick-up coil, and τ [s] is the integration time.

In the next step, the amplitude of BN (U_{bpp}), defined as the voltage difference between the maximum peak value of the magnetic BN (U_b) and the background noise (U_{ib}), was determined. Extended uncertainty was subsequently determined for the cast iron specimens with the shortest and longest cast iron flakes.

Fig. 2 General view of equipment for BN measurements: **a** Measuring head, and **b** schematic chart of its basic elements (1—tested specimen, 2—U-shaped core, 3—magnetizing coil, 4—core of the measuring coil, 5—measuring winding, 6—control winding) [17]



Moreover, an integral of the half-period voltage signal of BNM was calculated.

$$\text{Int}(U_b) = \int_{-U_{g \text{ max}}}^{+U_{g \text{ max}}} U_{sb} dU_g, \tag{2}$$

where:

$$U_{sb} = \sqrt{U_b^2 - U_{ib}^2}, \tag{3}$$

U_{sb} [V]—root mean square of the Barkhausen emission voltage after correction due to background noise, U_b [V]—root mean square of the coil output voltage, U_{ib} [V]—root mean square of background voltage, U_g [V]—generator voltage.

Also, the full width at half maximum (FWHM) of RMS envelope of BN was determined.

Subsequently, each of the specimen was polished in diamond suspension with granulation of 9 μm , 3 μm and 1 μm . Then, qualitative and quantitative analysis of the material's microstructure in the field of light microscopy was carried out. The quantitative analysis of one specimen included 200 measurement fields with a total area of 25.4mm². The area of single measurement field was 0.127 mm². The tests were performed using the planimetric method. The following geometric parameters for the flake graphite cast iron were determined:

- V_V [%] = A_A [%]—volume share of flake graphite is equal to the area volume according to the stereological relationship,
- \bar{N}_{LII} [1/mm]—number of precipitates per 1 mm of the incisal length in parallel direction,
- \bar{N}_L [1/mm] -number of precipitates per 1 mm of the incisal length in perpendicular direction,
- \bar{l}_{II} [μm]—minimum chord of the flake graphite,
- \bar{l} [μm]—maximum chord of the flake graphite,
- Ω —anisotropy coefficient of the flake graphite.

Nital etching was used to reveal the material microstructure, in order to observe the material's matrix.

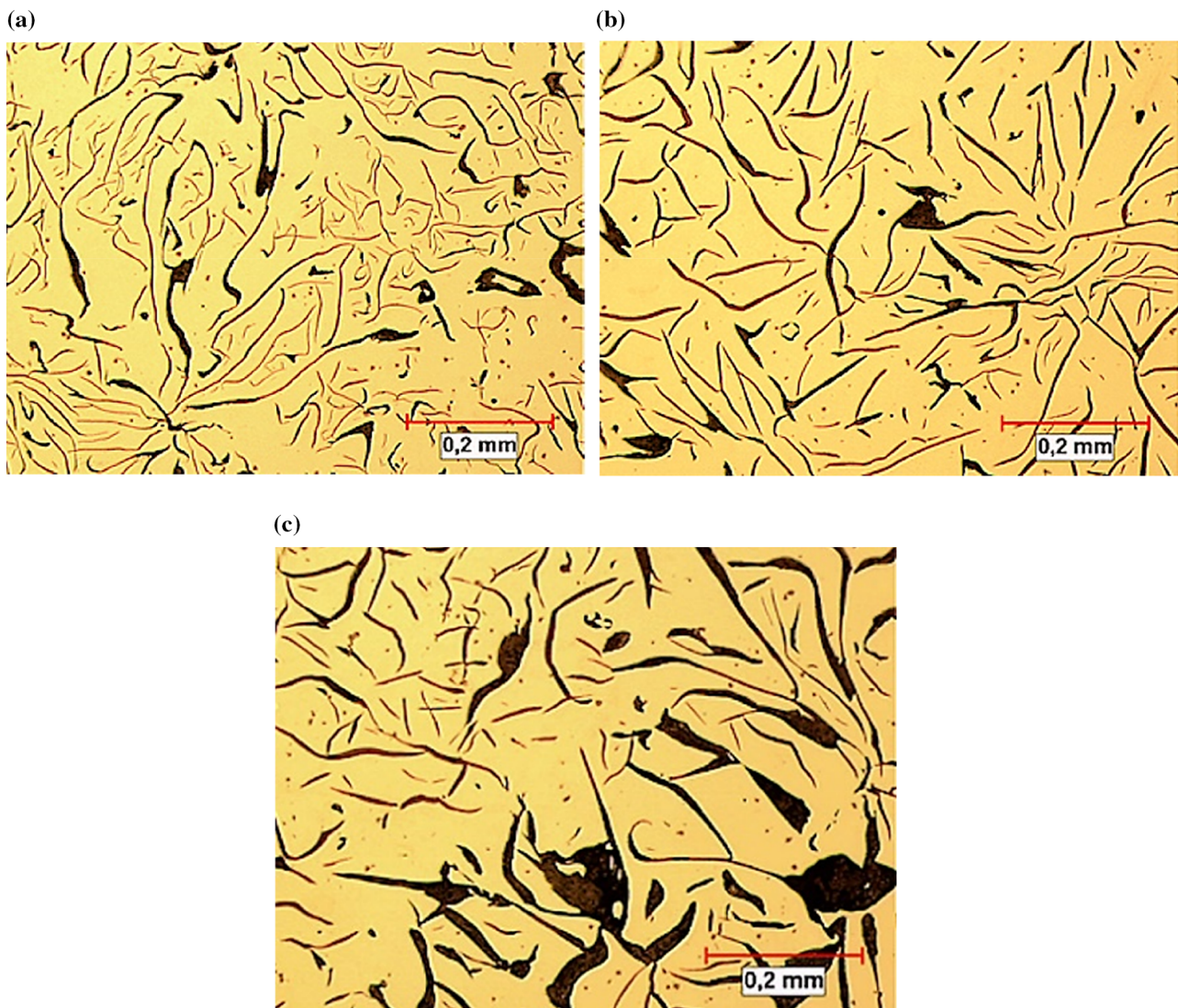


Fig. 3 **a** Specimen 3, $V_V = 14.27\%$, $\bar{l}_{II} = 7.31 \mu\text{m}$, mag. 100x. **b** Specimen 1, $V_V = 17.01\%$, $\bar{l}_{II} = 8.89 \mu\text{m}$, mag. 100x. **c** Specimen 6, $V_V = 17.47\%$, $\bar{l}_{II} = 9.41 \mu\text{m}$, mag. 100x

Finally, three measurements of Brinell hardness (HBW2.5/187.5) were carried out for each cast iron specimen. Expanded uncertainty was also calculated.

3 Results

As shown in Fig. 3a–c, the graphite shape has a full flake structure that varies in size. The nital etching revealed the pearlite structure of the material's matrix (Fig. 4). The geometric parameters of the graphite are summarized in Table 1 [27]. The results of the quantitative metallographic analysis indicate that the flake graphite (zig-zag lines) has the isotropic structure. The volume of the flake graphite ranged from 13.50% to 18.10% in the specimens tested. The flake

size ranged from 5.61 mm to 9.41 mm in a horizontal direction. In some areas of the brake disc, the graphite precipitates were therefore, about twice as large as the others. Taking into account \bar{N}_{LII} and \bar{N}_L parameters the graphite particles are uniformly distributed in the material matrix.

The RMS of BN envelopes are presented in Fig. 5. According to [28], the maximum of BN envelope comes from the ferrite plates in pearlite, while a slight increase in the effective voltage U_b at the generator voltage of about 2 V results from the volume of cementite plates in pearlite. Figure 6 shows the relationships between voltage and the microstructural parameters of the graphite precipitates. Linear relationships between BN amplitude and volume fraction, as well as BN amplitude and length of the flake graphite, were also found, Figs. 6a–7a. However, the integral from BN voltage turned out to be insensitive from both the volume fraction and

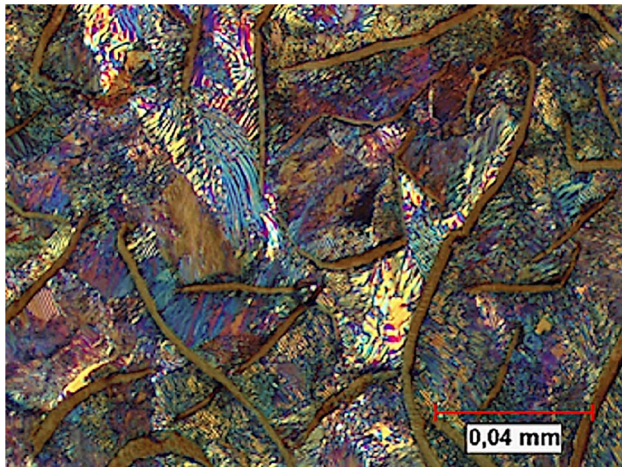


Fig. 4 The structure of the flake graphite (zig-zag lines) in pearlite matrix, specimen 10, etched state, phase contrast, mag. 500x

Table 1 Geometric parameters of the graphite

Specimen number		\bar{V}_v [%]	\bar{N}_{LII} [1/mm]	$\bar{N}_{L\perp}$ [1/mm]	\bar{l}_{II} [μm]	\bar{l}_{\perp} [μm]	Ω
1	w	17.01	116	117	8.89	8.77	1.000
	s	2.68	19	20	1.65	1.67	0.174
2	w	18.10	116	118	8.81	8.70	1.00
	s	2.77	19	20	1.58	1.60	0.170
3	w	14.27	142	143	7.31	7.29	1.01
	s	2.24	27	29	1.66	1.82	0.192
4	w	14.27	171	170	5.96	5.98	1.01
	s	1.63	25	24	0.996	0.948	0.128
5	w	15.48	159	162	6.50	6.38	0.987
	s	2.12	28	29	1.37	1.38	0.114
6	w	17.47	112	109	9.41	9.73	1.05
	s	3.44	27	28	2.46	2.57	0.197
7	w	16.55	142	139	7.46	7.64	1.03
	s	3.49	33	32	2.09	2.13	0.140
8	w	13.50	185	180	5.61	5.72	1.03
	s	2.19	34	32	1.18	1.15	0.138
9	w	15.35	172	171	5.93	6.00	1.02
	s	1.80	26	26	0.981	0.990	0.118
10	w	15.71	138	135	7.49	7.67	1.04
	s	2.27	23	24	1.52	1.65	0.186

w—average value; s—standard deviation

length of the flake graphite, Figs. 6b–7b. A linear relationship was also observed between the graphite volume and FWHM parameter, however, this magnetic parameter does not allow an estimation of the graphite flake size, Figs. 6c–7c.

The results of repeatability tests of BN for specimens with the shortest and longest graphite flake lengths are presented

in Figs. 8 and 9. For both specimen types, five measurements of BN level were carried out and extended uncertainty for all determined parameters was calculated, Tables 2, 3, 4. The expanded uncertainty was determined for the expansion factor $k_p = 2$, and confidence level of 95%.

Considering the integral from BN envelope, the specimens with the shortest and longest length of graphite flake were in the range of $0.44 \text{ V} \pm 0.02 \text{ V}$ and $0.37 \text{ V} \pm 0.05 \text{ V}$, respectively. The highest confidence interval was calculated for the FWHM parameter, Table 4. The greater expanded uncertainty for the specimen with the longest graphite flake length results from the fact that it had a higher volume of graphite flakes with more varied size.

The results of hardness measurements are presented in Table 5. The relationship between hardness and magnetic parameter is presented in Fig. 10. It was found, that the hardness of the iron slightly increases with the increase of BN amplitude, and that the hardness of specimen with the longer graphite flake length is lower than that of the cast iron specimen with the shortest graphite flake size.

4 Discussion

In order to clarify analysis, it should be emphasized that all specimens used in the experimental program had the lamellar structure for all microstructural components. Such features are relevant to both the flake graphite and pearlitic matrix of the material. However, as the graphite is diamagnetic, it did not contribute to BN level. Moreover, the BN did not come from the total pearlitic matrix of the material, but mostly from the ferritic plates in the pearlite. The cementite, as a weak magnetic, was not a decisive factor for the extent of domain walls pinning [29]. Therefore, taking into account the BN envelopes, one can observe only a slight increase of the envelope for $U_g = 2 \text{ V}$. On the other hand, the preferential orientation of lamellar ferrite in the pearlite may facilitate under magnetic field the passage of domain walls across a colony of boundaries in pearlitic grains. It has to be mentioned, that the reduction of ferrite and cementite plates thickness in the pearlite does not have significant effect on BN signal [30]. According to [31], the pearlite grains act as the nucleation sites for domains and serve as the pinning sites for domain walls. Simultaneously, the similar roles of nucleation and pinning sites are the result of the grain boundaries between pearlite and graphite.

The results obtained in this research, which show reduction of BN level with a size increase of the graphite precipitation, confirmed data presented in [21]. In both cases, the RMS amplitude of BN envelope changed linearly with respect to the size increase of the graphite precipitate. It should be noted, that in the case considered in this research the flake iron was investigated, however, in [21] the nodular

Fig. 5 RMS of BN envelopes for the brake disc; **a–j** the results for specimens distributed circumferentially in the middle of radius of the brake disc

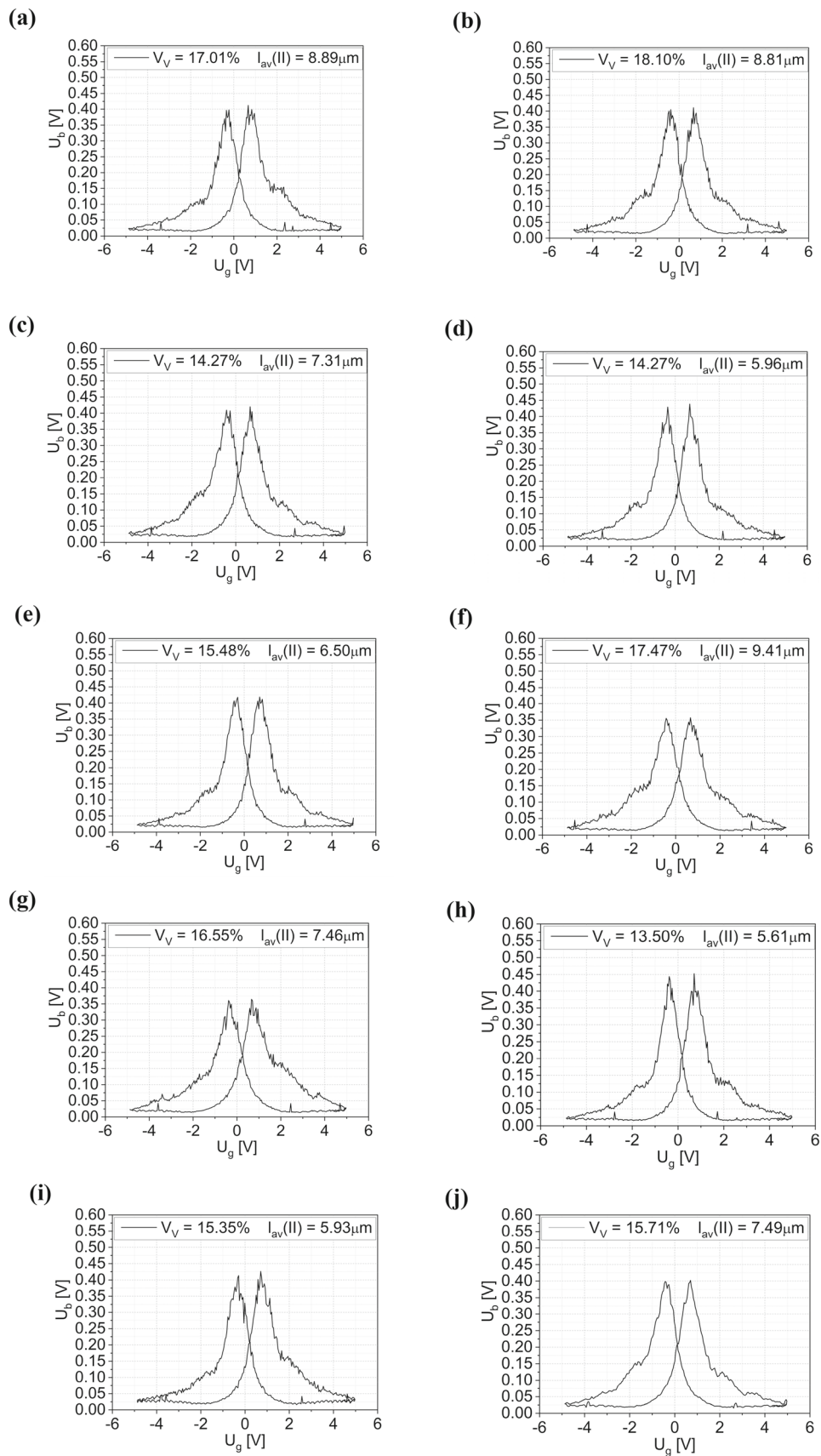


Fig. 6 **a** Amplitude of BN versus volume of flake graphite in the cast iron specimens. **b** Integral of BN versus volume of flake graphite in the cast iron specimens. **c** Full width at half maximum of the RMS of BN envelope versus volume of flake graphite in the cast iron specimen

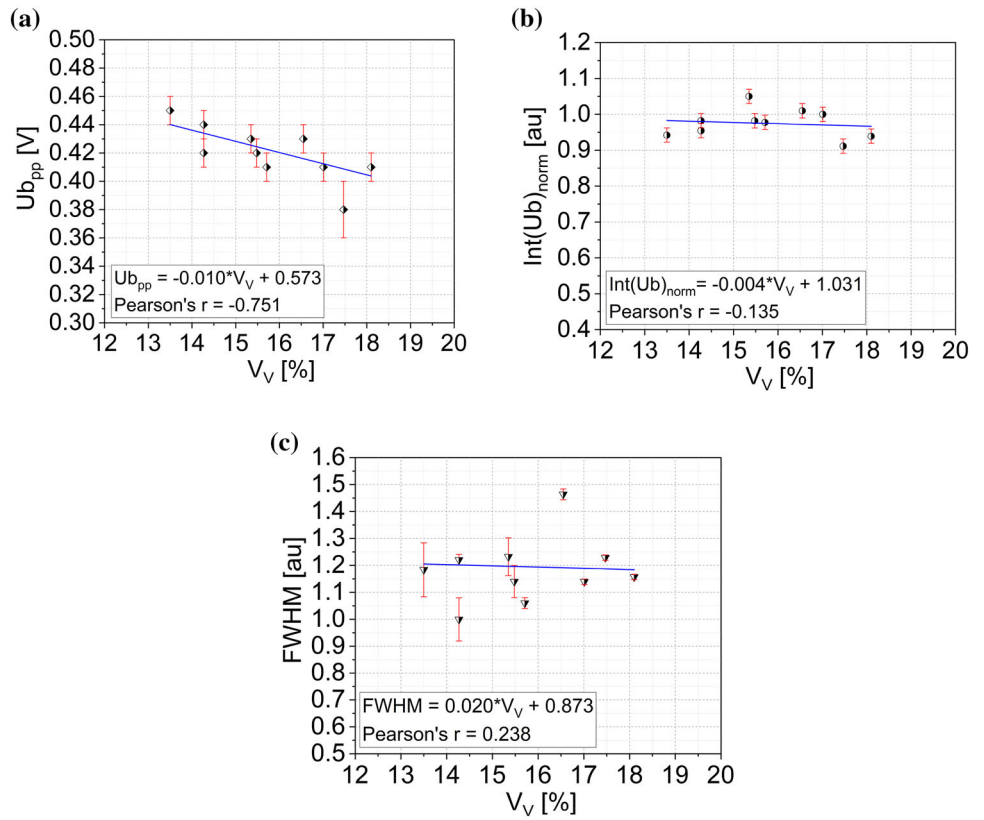
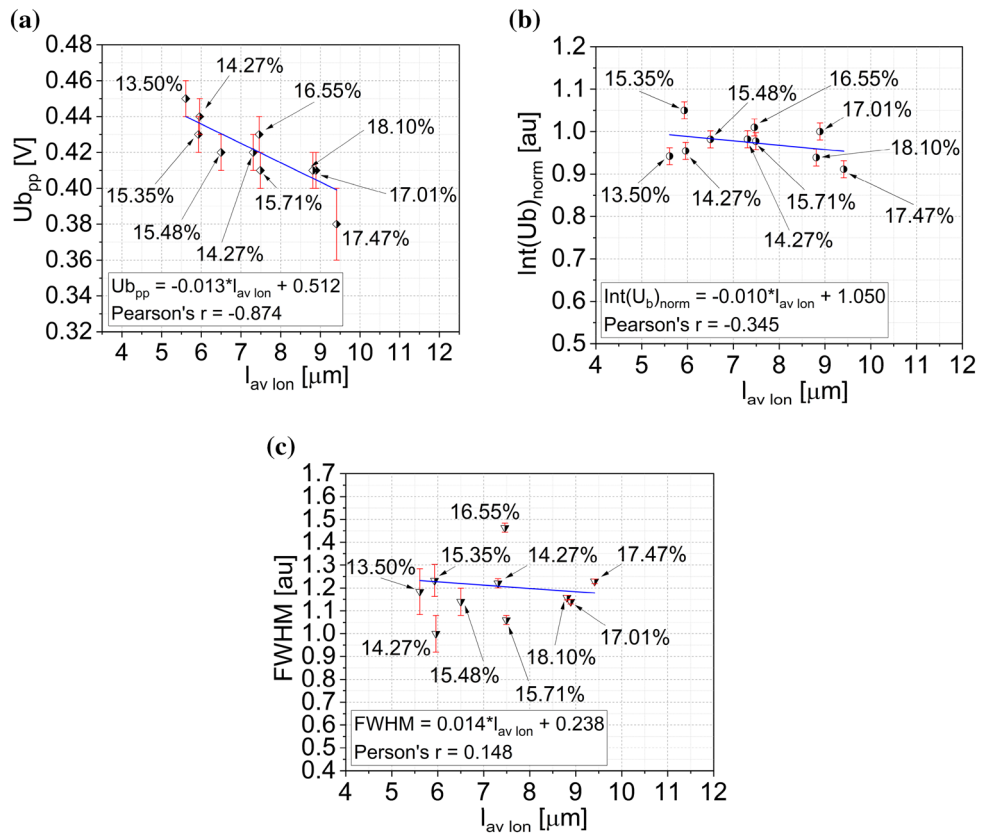


Fig. 7 **a** Amplitude of BN versus length of the graphite flake; the numbers in figure denote percentage volume of flake graphite in the cast iron specimens. **b** Integral of BN versus length of graphite flake; the numbers in figure denote percentage volume of flake graphite in the cast iron specimens. **c** Full width at half maximum of RMS envelope of BN versus length of the graphite flake; the numbers in the figure denote percentage volume of flake graphite in the cast iron specimens



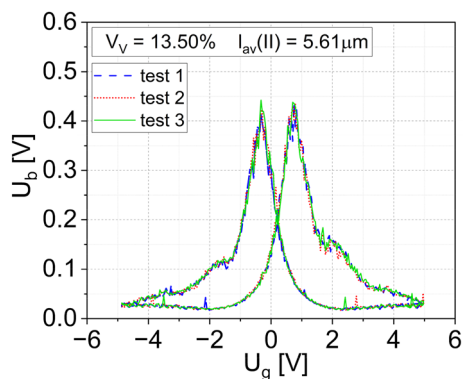


Fig. 8 Three tests to check repeatability of BN level for specimens with the shortest graphite flake

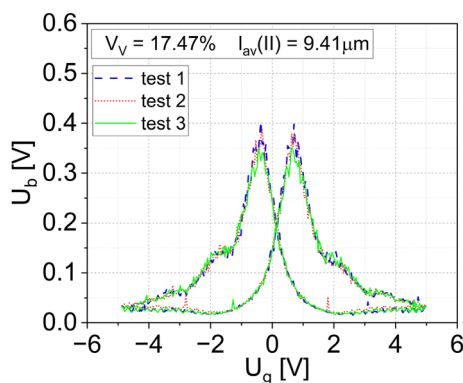


Fig. 9 Three tests to check repeatability of BN level for specimens with the longest graphite flake

cast iron was studied. The level of BN signal Ub_{pp} decreases. This is due to the fact, that if the greater graphite precipitations are, the greater barriers to the moving domain walls in the varying magnetic field strength take place. According to [21], such a linear relationship between the size of graphite precipitation and BN amplitude occurs up to the size of the graphite precipitation equal to 35 μm . When the size of secretion exceeds 35 μm , the signal level of BN increases. This is because the particles of graphite are too large to impede a movement of the domain walls [32]. Domain walls do not anchor on particles of the graphite.

Moreover, it was found that the inclination angle of the relationship $Ub_{pp} = f(l_{av})$ is similar to that presented in [32]. This is due to the fact that both materials have a fully pearlitic matrix. In [32] the relationship $Ub_{pp} = f(l_{av})$ for cast iron with ferritic and ferrite-pearlite matrix was also discussed. The same tendency of Ub_{pp} variation was found to decrease if l_{av} parameter was equal to 35 μm , for higher values of l_{av} , the Ub_{pp} started to increase. However, one can indicate that the angle of inclination in such cases is larger. This means that the domain wall's movement in the cast iron with pearlite matrix is more difficult, since the irregularities in form of the alternating ferrite and pearlite tiles are greater obstacles to domain walls than the ferrite or ferrite-pearlite matrix in the cast iron [10].

Unfortunately, according to [32] the cast iron hardness cannot be estimated based on BN parameters regardless of the type of material matrix. It was confirmed by the tests carried out for the pearlitic cast iron. The only exception is the cast iron with a pearlitic-cementite matrix, because it was found that as the hardness increases, the RMS voltage of

Table 2 The results of repeated measurements of BN amplitude

Size of the graphite flakes [μm]	Number of measurements of Ub_{pp} [V]					Average of Ub_{pp} [V]	Statistical parameter	
	(a)	(b)	(c)	(d)	(e)		Standard deviation	Expanded uncertainty [V]
$l_{min} = 5.61 \mu\text{m}$	0.45	0.44	0.44	0.44	0.45	0.44	0.01	± 0.02
$l_{max} = 9.41 \mu\text{m}$	0.35	0.35	0.38	0.39	0.40	0.37	0.02	± 0.05

Table 3 The results of repeated measurements of BN integral

Size of the graphite flakes [μm]	Number of measurements of $Int(Ub)_{norm}$ [au]					Average of $Int(Ub)_{norm}$ [au]	Statistical parameter	
	(a)	(b)	(c)	(d)	(e)		Standard deviation	Expanded uncertainty [au]
$l_{min} = 5.61 \mu\text{m}$	0.77	0.82	0.82	0.82	0.82	0.81	0.02	± 0.04
$l_{max} = 9.41 \mu\text{m}$	1.06	1.07	1.11	1.07	1.08	1.08	0.02	± 0.04

Table 4 The results of repeated measurements of the full width at half maximum of RMS of BN envelope

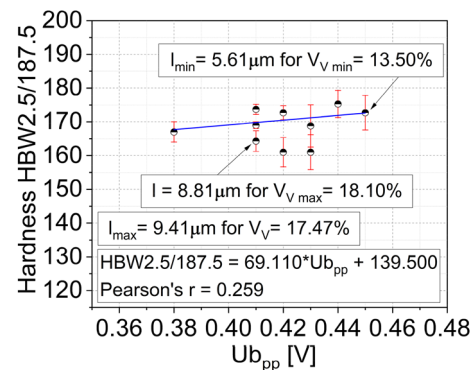
Size of the graphite flakes [μm]	Number of measurements of FWHM [au]					Average of FWHM [au]	Statistical parameter	
	(a)	(b)	(c)	(d)	(e)		Standard deviation	Expanded uncertainty [au]
$l_{\min} = 5.61 \mu\text{m}$	0.74	0.74	0.73	0.73	0.75	0.74	0.01	± 0.02
$l_{\max} = 9.41 \mu\text{m}$	1.18	1.38	1.25	1.17	1.13	1.22	0.10	± 0.24

Table 5 Hardness measurements of the cast iron specimens

Number of measurements	1	2	3	4	5	6	7	8	9	10
1	169	165	156	179	171	170	171	177	167	174
2	168	161	163	176	175	164	174	167	158	175
3	170	167	164	171	172	167	162	174	158	172
Average hardness	169.0	164.3	161.0	175.3	172.7	167.0	168.8	172.7	161.0	173.7
Standard deviation	1.00	3.06	4.36	4.04	2.08	3.00	6.25	5.13	5.20	1.53
Expanded uncertainty	± 2.00	± 6.11	± 8.72	± 8.09	± 4.17	± 6.00	± 12.49	± 10.27	± 10.39	± 3.06

BN also increases [32]. In general, the hardness tests carried out on the brake disc specimens did not show a significant scatter of data, which should be considered as a satisfactory result. This provides evidence for a roughly homogeneous microstructure of the sample tested, which in turn proves the lack of technological defects of the material in question.

The reason for the widespread usage of BNM is connected with the satisfactory repeatability of the results. The main problem in BN measurement is controlling of the magnetizing conditions. Magnetization might be too weak for example, and therefore, it is not possible to obtain a properly shaped BN envelope. Moreover, an incidental air gap may occur between the yoke and specimen, and as a consequence, the possibility to record the Barkhausen effect diminishes. Since the domain wall's movement needs to be detected, the pick-up coil plays a very important role. Both, the accuracy and repeatability of the results depend on the calibration and detection of the Barkhausen pulses. It was found [33], that the number of turns in detection of the coil affects the shape of the amplitude peaks of BN. Such feature was observed for a low magnetic field when the amplitude of BN increased with increasing the winding of the detection coil [33]. Measurement uncertainty may be also dependent on the other factors. Among them one can indicate an indirect measurements of the magnetic field distribution as well as its variation in time [34]. In the case of a well-defined magnetic field, the procedure of the basic parameters determination, which come from RMS of BN envelopes such as height, width and peak location with respect to the magnetic flux density B of dB/dt

**Fig. 10** Relationship between hardness and BN for the flake graphite cast iron

brings some doubts [34] related directly to the possible material inhomogeneity [35]. As a consequence, the measuring head can be positioned in places which are not able to reflect accurately the inhomogeneously of distributed precipitates in the material matrix or nonuniformly distributed impurities in the material tested.

5 Conclusions

The paper presents application opportunities of the magnetic technique supporting microscopic analysis of the structural elements manufactured using the gray cast iron. The brake disc made of the gray cast iron with different sizes of graphite flakes was selected for tests with the focus on analysis

of hardness and BN parameters and their mutual relationships. Since the hardness of the cast iron depends mainly on the material matrix, only slight differences in the hardness of specimens with varying sizes of graphite flakes were observed. It has to be emphasised, that BN effect can be successfully used to assess a size of the graphite particles in the cast iron. More importantly, BNM can be expanded and potentially applied to estimate a size of the graphite precipitates in accordance with the ISO945-1:2019 [36], replacing conventional metallographic tests.

Acknowledgements Not applicable.

Author Contributions Conceptualization: KM, Metodology: KM, Formal analysis: KM, Investigation: KM, Data curation: KM, ZLK, Writing—original draft: KM, ZLK, Writing – review & editing: ZLK, Supervision: ZLK, Project administration: KM, Funding acquisition: KM. All authors have read and agreed to publish the manuscript.

Funding Not applicable.

Data Availability The data sets generated and/or analysed during the current study are not publicly available due [PROJECT RESULTS FOR A MANUFACTURER] but are available from the corresponding author on request.

Declarations

Competing Interests The authors have no competing interest to declare are relevant to the content of this article.

Ethical Approval Not applicable (no human participants, human data or human tissues and/or animals were involved in this as the objects of research).

Consent for Publication Not applicable.

Open Assess Not applicable.

Open Access This article is licensed under a Creative Commons Attribution 4.0 International License, which permits use, sharing, adaptation, distribution and reproduction in any medium or format, as long as you give appropriate credit to the original author(s) and the source, provide a link to the Creative Commons licence, and indicate if changes were made. The images or other third party material in this article are included in the article's Creative Commons licence, unless indicated otherwise in a credit line to the material. If material is not included in the article's Creative Commons licence and your intended use is not permitted by statutory regulation or exceeds the permitted use, you will need to obtain permission directly from the copyright holder. To view a copy of this licence, visit <http://creativecommons.org/licenses/by/4.0/>.

References

- Masaud, I.M., Al-Jarrah, J.A., Abu Mansour, T.: Manufacturing of gray cast iron automotive disc brake. *Ind. J. Appl. Res.* **4**, 129–131 (2014)
- Polak, A., Grzybek, J.: The mechanism of changes in the surface layer of grey cast iron automotive brake disc. *Mater. Res.* **8**, 475–479 (2005). <https://doi.org/10.1590/S1516-14392005000400020>
- Walton, C.F., Opar, T.J.: Iron casting handbook. Iron Casting Society Inc, New York (1981)
- Konoplyuk, S., Abe, T., Uchimoto, T., Takogi, T., Kurosawa, M.: Characterization of ductile cast iron by eddy current method. *NDT E Int.* **38**, 623–626 (2005). <https://doi.org/10.1016/j.ndteint.2005.02.008>
- Encyclopedia of Modern Physics [in Polish] PWN, Warszawa (1983)
- Piech, T.: Magnetic research. The use of the Barkhausen effect [in Polish]. Biuro Gamma, Warszawa (1998)
- Jiles, D.: Introduction to magnetism and magnetic materials. Taylor and Francis Group, New York (1998)
- Blaow, A., Evans, J.T., Shaw, B.A.: The effect of microstructure and applied stress on magnetic Barkhausen emission in induction hardened steel. *J. Mater. Sci.* **42**, 4364–4371 (2007). <https://doi.org/10.1007/s10853-006-0631-5>
- O'Sullivan, D., Cotterell, M., Cassidy, S., Tanner, D.A., Mészáros, I.: Magneto-acoustic emission for the characterisation of ferritic stainless steel microstructural state. *J. Magn. Magn. Mater.* **271**, 381–389 (2004). <https://doi.org/10.1016/j.jmmm.2003.10.004>
- Saquet, O., Chicois, J., Vincent, A.: Barkhausen noise from plan carbon steel: analysis of the influence of microstructure. *Mat. Sci. Eng. A* **269**, 73–82 (1999). [https://doi.org/10.1016/S0921-5093\(99\)00155-0](https://doi.org/10.1016/S0921-5093(99)00155-0)
- Davut, K.: Characterization of steel microstructures by magnetic Barkhausen noise technique. MS Thesis, Middle East Technical University, Ankara (2006)
- Kleber, X., Hug-Amalric, A., Merlin, J.: Evaluation of proportion of phases and mechanical strength of two-phase steels using Barkhausen noise measurements: application to commercial dual-phase steel. *Metall. Mater. Trans. A* **39**, 1308–1318 (2008). <https://doi.org/10.1007/s11661-008-9508-3>
- Davut, K., Gür, C.H.: Monitoring the microstructural evolution in spheroidized steels by magnetic Barkhausen noise measurements. *J. Nondestruct. Eval.* **29**, 241–247 (2010). <https://doi.org/10.1007/s10921-010-0082-4>
- Yamuara, S., Furuya, Y., Watanabe, T.: The effect of grain boundary microstructure on Barkhausen noise in ferromagnetic materials. *Acta Mater.* **49**, 3019–3027 (2001). [https://doi.org/10.1016/S1359-6454\(01\)00189-6](https://doi.org/10.1016/S1359-6454(01)00189-6)
- Akçaoğlu, F., Gür, C.H.: Monitoring magnetic anisotropy variations in cold-rolled steels by magnetic Barkhausen noise, 11th European conference on non-destructive testing (ECNDT 2014), October 6–10. Prague, Czech Republic. (2014) https://www.ndt.net/events/ECNDT2014/app/content/Paper/458_Gur_Rev1.pdf
- Mohopatra, J.N., Ray, A.K., Swaminathan, J., Mitra, A.: Creep behavior study of virgin and service exposed 5Cr-0.5Mo steel using magnetic Barkhausen emissions technique. *J. Magn. Magn. Mater.* **320**, 2284–2290 (2008)
- Makowska, K., Kowalewski, Z.L., Augustyniak, B., Piotrowski, L.: Determination of mechanical properties of P91 steel by means of magnetic Barkhausen emission. *J. Theor. Appl. Mech.* **52**, 181–188 (2014)
- Makowska, K., Kowalewski, Z.L.: Variation of Barkhausen noise, magnetic and crystal structure of ferromagnetic medium-carbon steel after different loading processes. *Phys. MetMetallogr.* **121**, 115–122 (2020)
- Gür, C.H., Kiliçli V., Erdogan, M.: Investigation the austempering parameters of ductile iron by magnetic Barkhausen noise technique, 17th World Conference on Nondestructive testing, Shanghai, China, 25–28 October. (2008) <https://www.ndt.net/article/wcndt2008/papers/473.pdf>
- Kiliçli, V., Yalçın A., Davut, K.: Non-destructive determination of pearlite content of ductile iron castings by magnetic Barkhausen

- Noise Analysis Technique, 19th International Metallurgy & Materials Congress, 1–4. (2018) <https://www.semanticscholar.org/paper/Non-Destructive-Determination-of-Pearlite-Content-Kilicli-Yalcin/e3b46b1e4f2242b343d4a2549f32a1bad1cfeb9c>
21. Stupakov, O., Uchimoto, T., Takagi, T., Sanaee, S.A., Tomás, I.: Evaluation of ductile cast iron microstructure by magnetic hysteresis and Barkhausen noise method. *St Appl. ElecMech. Electr. Nondestruct. Eval.* **32**, 232–239 (2009). <https://doi.org/10.3233/978-1-60750-023-0-232>
 22. Hetherington, M.G., Jakubovics, J.P., Szpunar, J.A., Tanner, B.K.: High-voltage Lorentz electron microscopy studies of domain structures and magnetization processes in pearlitic steels. *Phil. Mag.* **B56**, 561–577 (1987). <https://doi.org/10.1080/13642818708220163>
 23. Gür, C.H., Ozer, M., Erdogan, M.: Investigation of the variations in microstructure and mechanical properties of dual-matrix ductile iron by magnetic Barkhausen noise analysis. *ResNondestr. Eval.* **19**, 44–60 (2008). <https://doi.org/10.1080/09349840701635278>
 24. Altpeter, I.: Nondestructive evaluation of cementite content in steel and white cast iron using inductive Barkhausen noise. *J. Nondestruct. Eval.* **15**, 45–60 (1996)
 25. Buttle, D.J., Scruby, C.B., Jakubovics, J.P., Briggs, G.A.D.: Magneto-acoustic and Barkhausen emission: their dependence on dislocations in iron. *Phil. Mag. A* **55**, 717–734 (1987). <https://doi.org/10.1080/01418618708214379>
 26. Dudziewicz, J.: Fundamentals of electromagnetism [in Polish]. WNT, Warsaw (1972)
 27. Ryś, J.: Stereology of materials [in Polish], Fotobit Design, Kraków (1995)
 28. Altpeter, I., Becker, R., Dobmann, G., Kern, R., Theiner, W., Yashan, A.: Robust solutions of inverse problems in electromagnetic non-destructive evaluation. *Invers. Problems* **18**, 1907–1921 (2002). <https://doi.org/10.1088/0266-5611/18/6/328>
 29. Gür, C.H., Çam, İ: Comparison of magnetic Barkhausen noise and ultrasonic velocity measurement for microstructure evaluation of SAE 1040 and SAE 4140 steels. *Mater. Char.* **58**, 447–452 (2007). <https://doi.org/10.1016/j.matchar.2006.06.008>
 30. Clapton, L., Jagadish, C., Atherton, D.L.: The influence of pearlite on Barkhausen noise generation in plain carbon steels. *Acta Met. Mater.* **39**, 1555–1562 (1991). [https://doi.org/10.1016/0956-7151\(91\)90242-S](https://doi.org/10.1016/0956-7151(91)90242-S)
 31. Lo, C.C.H., Lee, S.J., Kerdus, L.C., Jiles, D.C.: Examination of the relationship between the parameters of Barkhausen effect model and microstructure of magnetic materials. *J. Appl. Phys.* **91**, 7651–7654 (2002). <https://doi.org/10.1063/1.1453312>
 32. D’Amato, C., Verdu, C., Kleber, X., Regheere, G., Vincent, A.: Characterization of austempered ductile iron through Barkhausen noise measurements. *J. Nondestruct. Eval.* **22**, 127–139 (2003). <https://doi.org/10.1023/B:JONE.0000022032.66648.c5>
 33. Blaow, M.M., Shaw, B.A.: Magnetic Barkhausen noise profile analysis: effect of excitation field strength and detection coil sensitivity in case carburized steel. *Mat. Sci. Appl.* **5**, 258–266 (2014). <https://doi.org/10.4236/msa.2014.55030>
 34. Augustyniak, M., Augustyniak, B., Piotrowski, O.L., Chmielewski, M.: Determination conditions in a double-core Barkhausen noise measurement set-up. *J. Nondestruct. Eval.* **34**, 1–8 (2015). <https://doi.org/10.1007/s10921-015-0288-6>
 35. Santa-aho, S., Laitinen, A., Sorsa, A., Vippola, M.: Barkhausen noise probes and modelling: a review. *J. Nondestruct. Eval.* **38**, 1–11 (2018). <https://doi.org/10.1007/s10921-019-0636-z>
 36. Microstructure of cast irons -- Part 1: Graphite classification by visual analysis (ISO 945–1:2019)

Publisher’s Note Springer Nature remains neutral with regard to jurisdictional claims in published maps and institutional affiliations.